THE NONLINEAR RESPONSE OF CRACKED ALUMINUM SHELLS SUBJECTED TO COMBINED LOADS

Cheryl A. Rose,[*] Richard D. Young,[*] and James H. Starnes, Jr.[†]
NASA Langley Research Center
Hampton, Virginia 23681-2199

Abstract

The results of a numerical study of the nonlinear response of thin unstiffened aluminum cylindrical shells with a longitudinal crack are presented. The shells are analyzed with a nonlinear shell analysis code that accurately accounts for global and structural response phenomena. The effects of initial crack length on the prebuckling, buckling and postbuckling responses of a typical shell subjected to axial compression loads, and subjected to combined internal pressure and axial compression loads are described. Both elastic and elastic-plastic analyses are conducted. Numerical results for a fixed initial crack length indicate that the buckling load decreases as the crack length increases for a given pressure load, and that the buckling load increases as the internal pressure load increases for a given crack length. Furthermore, results indicate that predictions from an elastic analysis for the initial buckling load of a cracked shell subjected to combined axial compression and internal pressure loads can be unconservative. In addition, the effect of crack extension on the initial buckling load is presented.

Introduction

The fail-safe design philosophy, when applied to transport aircraft fuselage structure, requires that these structures retain adequate structural integrity in the presence of discrete-source damage or fatigue cracks. One type of damage frequently associated with the structural integrity of fuselage shell structures is a longitudinal crack in the fuselage skin that is subjected to circumferential stresses resulting from the internal pressure loads, and to axial stresses resulting from the vertical bending and shearing of the fuselage that are induced by normal flight loads. The structural response of a transport fuselage structure with a crack is influenced by the local stress and displacement gradients near the crack and by the internal load distribution in the shell. Local fuselage out-of-plane skin displacements near a crack can be large compared to the fuselage skin thickness, and these displacements can couple with the internal stress resultants in the shell to amplify the magnitudes of the local stresses and displacements near the crack. In addition, the stiffness and internal load distributions in a shell with a crack will change as the crack grows and when the skin buckles, and these changes will affect the local stress and displacement gradients near the crack. Furthermore, crack growth may influence shell buckling, and shell buckling may influence crack growth. This compound nonlinear response and interaction must be understood and predicted accurately in order to determine the structural integrity and residual strength of current fuselage structures with damage, and to develop more efficient damage tolerant designs for future aerospace structures.

Recent studies (e.g., Refs. 1-4) have shown that the structural response and structural integrity of a shell with a crack can be studied analytically with a nonlinear structural analysis procedure that can model crack growth in the shell. The magnitudes of the mechanical loads used in these studies are representative of loads that do not buckle the skin of the fuselage. To maximize structural efficiency, fuselage shells are usually designed to allow the fuselage skin to buckle above a specified design load that is less than the design limit load for the shell. During the design of the fuselage, it is assumed that the design limit load can occur anytime during the service life of the aircraft. As a result, a long crack could exist in the fuselage shell after a considerable amount of flight service, and loading conditions could occur that cause the shell with the long crack to buckle. These cracks can act as effective geometric imperfections and significantly reduce the load carrying capacity of the shell.

Most nonlinear-response and residual-strength analyses that have been conducted to date for fuselage shells with long cracks have been limited to an unbuckled fuselage shell response.[1-4] Recently, nonlinear numerical and experimental studies of the effects of longitudinal cracks on the nonlinear response of thin, unstiffened laboratory-scale aluminum cylindrical shells subjected to internal pressure loads and axial compression loads indicate that the behavior of a shell can be influenced significantly by the initial length of the crack.[5-7] In particular, the effect of initial crack length on the initiation of stable tearing and unstable crack growth in a

[*]Aerospace Engineer, Mechanics and Durability Branch. Member, AIAA.
[†]Chief Engineer, Structures and Materials Competency. Fellow, AIAA.

typical shell subjected to internal pressure loading was predicted using elastic-plastic finite-element analyses. The results of these analyses indicate that the pressure required to initiate stable and unstable tearing in a shell subjected to internal pressure decreases as the crack length increases. In addition, the effects of crack length on the prebuckling, buckling, and postbuckling responses of a typical shell subjected to axial compression were predicted using elastic finite-element analyses. The results of these analyses indicate that a crack in a shell structure subjected to axial compression loads can cause a significant reduction in the buckling load of the shell, and that the initial buckling loads decrease as the crack length increases. Furthermore, the initial local postbuckling response near the crack is characterized by large local deformations and stresses, which may cause the material to yield locally, and is not accurately represented by an elastic analysis.[6] In addition, studies of the elastic response of cylindrical shells with longitudinal cracks and subjected to internal pressure and axial compression loads, e.g., Ref. 5, indicate that the interaction between the internal pressure and axial compression loads can have a significant effect on the local response of the shell.

The present paper extends the studies described above by including the effect of nonlinear material behavior on the numerical buckling response predictions of thin, unstiffened, laboratory scale, aluminum shells with centrally located longitudinal cracks and subjected to internal pressure and axial compression loads. The internal-pressure level is varied to determine the effects of crack length and the magnitude of the internal pressure load on the response of these shells. In addition, the interaction between crack extension and initial local buckling is addressed; that is, the cracks are allowed to grow along a predefined path during the stability analysis. Geometric parameters varied in the study include the shell wall thickness and the initial crack length. Predicted prebuckling, buckling, and postbuckling results of material linear and material nonlinear analyses are presented and compared for cylindrical shells subjected to axial compression loads and combined internal pressure and axial compression loads. The results presented demonstrate the influence of the loading condition and initial crack length on shell buckling instabilities.

Shell Geometry and Analysis Procedure

Shell Geometry

The geometry of the shells analyzed in this study is defined in Fig. 1. The shells have a 9.0-inch radius, R, a 0.020- or 0.040-inch-thick wall, t, and a 36.0-inch length, L. A longitudinal crack is located at $\theta = 0°$ and at shell midlength. The initial crack length, a, ranges from 1.0 to 4.0 inches. The shells are typical laboratory-scale

cylindrical shells and are made of 2024-T3 aluminum alloy with the sheet rolling direction oriented in the circumferential direction. A piecewise linear representation was used for the uniaxial stress-strain curve for 2024-T3 aluminum (Fig. 2).[8] The Young's modulus and Poisson's ratio of the material are 10.35 msi, and 0.30, respectively. The loading conditions for the shells consists of axial compression loads and combined internal pressure and axial compression loads.

Nonlinear Analysis Procedure

The shell responses were predicted numerically using the STAGS (STructural Analysis of General Shells) nonlinear shell analysis code.[9] STAGS analysis capabilities include stress, nonlinear response, stability, vibration and transient response analyses, with both material and geometric nonlinearities represented. The code uses both the modified and full Newton methods for its nonlinear solution algorithms, and accounts for large rotations in a shell by using a co-rotational algorithm at the element level. The Riks pseudo arc-length path following method[10,11] is used to continue a solution past limit points in a nonlinear response. For situations where the standard arc-length method fails to converge to solutions beyond instability points, a nonlinear transient analysis method can be used.[12] The transient analysis option in STAGS uses proportional structural damping and an implicit numerical time-integration method developed by Park.[13]

STAGS can also perform crack-propagation analyses, and can represent the effects of crack growth on nonlinear shell response. A nodal release method and a load-relaxation technique are used to extend a crack while the shell is in a nonlinear equilibrium state.[14] The condition for crack extension is based on a fracture criterion. When a crack is to be extended, the forces necessary to hold the current crack-tip nodes together are calculated. The crack is extended by releasing the nodal compatibility condition at the crack tip, applying the equivalent crack-tip forces, and then releasing these forces to establish a new equilibrium state, which corresponds to the longer crack. The changes in the stiffness matrix and the internal load distribution that occur during crack growth are accounted for in the analysis, and the nonlinear coupling between the internal forces and in-plane and out-of-plane displacement gradients that occurs in a shell are properly represented. Output from STAGS, associated with a crack, includes the strain-energy-release rate in an elastic analysis, and the crack-tip-opening angle (CTOA) in a material nonlinear analysis.[2,14] These quantities can then be used as part of a fracture criterion in an elastic analysis or a material nonlinear analysis to predict the stable crack growth behavior and residual strength of a damaged shell.

Typical finite element models used to simulate the response of the cracked shells are shown in Fig. 3. The models shown in Fig. 3a were used for analyses of the axial compression and combined axial compression and internal pressure load cases, respectively, when the interaction between crack extension and local buckling was not addressed; that is, the material was assumed to be infinitely tough and crack propagation during loading was not considered. The finite element model shown in Fig. 3b was used for the combined load case to study the interaction between crack extension and local buckling. Cracks with initial lengths of 1.0 to 4.0 inches were defined in the model along $\theta = 0°$. Straight cracks were assumed, so that crack extension was self-similar. Mesh refinement was used to provide elements with side lengths equal to 0.040 inches along the line of crack extension. This mesh density was required to predict accurately the yielding at the crack tip and crack extension using the critical CTOA fracture criterion.[15]

The shells were modeled using STAGS standard 410 quadrilateral shell elements, and 510 and 710 mesh-transition elements, where needed. The elements are flat facet-type elements and are based on Kirchoff-Love shell theory and the nonlinear Lagrangian strain tensor.[9,16] Each of the shell element nodes has six degrees of freedom, including three translational degrees of freedom, u, v, and w, and three rotational degrees of freedom, ru, rv, and rw about the axes x, y, and z, respectively (see Fig. 3). Radial and circumferential translational and rotational displacement constraints were imposed on the ends of the shells during the load application.

The loading conditions on the shells included axial compression and combined axial compression and internal pressure loads. For the case of an axial compression load only, the compression load was applied to the ends of the shell by specifying a uniform end displacement. For the combined internal pressure and axial compression load cases, a live internal pressure load was applied to the shell first and then increased until the desired load level was obtained. After this load level was attained, an increasing axial compression load was applied. The internal pressure load was simulated by applying a uniform lateral pressure to the shell wall and by applying an axial tensile force to account for bulkhead pressure loads to the ends of the shell. Multi-point constraints were used to enforce a uniform end displacement. The axial compression load for the combined load case was applied to the ends of the shell by specifying an additional axial force while retaining the multi-point constraints to enforce a uniform end displacement.

Both elastic and elastic-plastic analyses were conducted. For the elastic-plastic analyses the material non-linearity was represented by the White-Besseling[17,18] or mechanical sub-layer model, distortional-energy plastic-

ity theory available in STAGS. The critical crack-tip-opening angle (CTOA) fracture criterion[8,15] was used to simulate stable crack growth for the combined load case analyses in which crack extension was considered. The critical CTOA criterion uses the crack opening angle as the fracture parameter. The CTOA, evaluated at a fixed distance from the moving crack tip, is defined as the angle made by the upper crack surface, the crack tip, and the lower crack surface. In the present study, the CTOA was evaluated at a distance of 0.04 inches behind the crack tip. Newman[15] has shown this distance to be adequate for analyzing stable crack growth in a variety of materials. The criterion assumes that crack growth will occur when the angle reaches a critical value, $CTOA_{cr}$, and that the critical value will remain constant as the crack extends. The value of the critical angle is dependent on the sheet material, the sheet thickness, and the crack orientation relative to the rolling direction. The critical angle for a particular material and thickness can be obtained by numerically simulating the fracture behavior of a laboratory specimen, using an elastic-plastic analysis, and determining the angle that best describes the experimentally observed fracture behavior. The critical angle of 5.36° used in the present study was determined by matching STAGS predictions, for the fracture behavior of a shell with the geometry described above and with a 4.0-inch-long longitudinal crack, with the experimentally observed behavior of an aluminum shell of the same geometry and subjected to internal pressure loads.

The prebuckling, buckling, and postbuckling responses of the shells were determined using a combination of the quasi-static and transient analysis capabilities available in STAGS. The prebuckling responses and some postbuckling responses were determined using the standard arclength projection method available in STAGS. For cases where convergence difficulties were encountered beyond instability points using the standard arclength method, the transient analysis option of the code was used. The transient analysis was initiated at an unstable equilibrium state just beyond the instability point by applying an increment to the end-shortening displacement. The transient analysis was continued until the kinetic energy in the system damped out to a negligible level. A load relaxation procedure was then applied to the system to establish a stable equilibrium state. The subsequent stable postbuckling response of the shell was computed using a standard nonlinear, quasi-static analysis.

Results and Discussion

The nonlinear analysis results for thin unstiffened aluminum cylindrical shells with a longitudinal crack are presented in this section. Results have been generated

for two loading conditions: axial compression load only, and combined internal pressure and axial compression loads. Results for these loading conditions are presented for shells with a longitudinal crack at shell midlength and with initial crack lengths of 1.0, 2.0, 3.0 and 4.0 inches. For the axial compression loading case, the axial compression load was increased from zero to the maximum axial load that the shell could support. An initial outward geometric imperfection, in the form of the lowest eigenmode, was used in all of the nonlinear analyses for axial compression loads to initiate local deformations in the vicinity of the crack. For the combined internal pressure and axial compression loading cases, a live internal pressure load was applied to the shell first and then increased until the desired load level was obtained. After this load level was attained, an increasing axial compression load was applied. Results have been generated for internal pressure load levels of 10.0, 30.0, and 50.0 psi. Shells with both 0.020- and 0.040-inch wall thicknesses were considered for the axial compression load case, but only shells with a 0.040-inch wall thickness were considered for the combined internal pressure and axial compression load case. Typical results are presented to illustrate the effects of crack length and internal pressure load level on the prebuckling, buckling and postbuckling responses of a shell subjected to axial compression loads, and combined internal pressure and axial compression loads. The effect of material nonlinear behavior on the response predictions is also assessed.

<u>Axial Compression Loads</u>

Results for 0.020- and 0.040-inch-thick aluminum shells with initial crack lengths of 1.0, 2.0, 3.0 and 4.0 inches are presented in Figs. 4-17 to identify typical response characteristics of a compression loaded shell with a longitudinal through crack. Predicted load shortening response curves and load-radial displacement response curves for shells with 1.0-, 2.0-, 3.0-, and 4.0-inch-long cracks are provided in Figs. 4a-7a, and Figs. 4b-7b, respectively, to demonstrate the overall compression response of the shells. Results for the 0.040-inch-thick shell are presented in Figs. 4 and 5 and results for the 0.020-inch-thick shell are presented in Figs. 6 and 7. The applied compression and end-shortening values are normalized by the corresponding classical buckling values for a shell without a crack, and the radial displacement at the crack center is normalized by the shell wall thickness, t.

The results in Figs. 4-7 indicate that the overall compression response predicted from both the elastic and elastic-plastic analyses is qualitatively the same for the 0.020- and 0.040-inch-thick shells, and is dependent on the initial crack length. For the 0.020- and 0.040-inch-thick shells with a 1.0-inch-long crack, the crack in-

troduces an effective imperfection that causes general instability to occur at the load indicated by the X on the curves for a shell with a 1.0-inch-long crack in Figs. 4a-7a. These shells cannot support additional compression load after buckling. For a shell with a longer crack, local buckling near the crack precedes shell collapse. The open symbols in Figs. 4a-7a identify the loads that correspond to initial local buckling near the crack for the 0.040-inch-thick shell with the 2.0-, 3.0-, and 4.0-inch-long initial cracks, and for the 0.020-inch-thick shell with the 2.0-, and 3.0-inch-long initial cracks. The local crack prebuckling and buckling responses are qualitatively similar to the response of plates loaded in compression. The predictions from an elastic and an elastic-plastic analysis, respectively, for the normalized radial displacement w_o/t at the center of the crack edges for the 0.040-inch-thick shell are shown in Figs. 4b and 5b. The corresponding predictions for the 0.020-inch-thick shell are shown in Figs. 6b and 7b. Prior to buckling the radial displacement w_o at the center of the crack edges is nearly equal to zero. Once the critical load is reached, w_o increases rapidly with increase in load. Initial local buckling is followed by a stable postbuckling response, and the load can be further increased after local buckling has occurred near the crack edges.

As the load is increased after initial local buckling has occurred, the 0.040-inch-thick shell with the 2.0-inch-long crack, collapse, as indicated by the X on the curve for a shell with a 2.0-inch-long crack in Figs. 4a and 5a. The 0.040-inch-thick shells with the 3.0- and 4.0-inch-long cracks, and the 0.020-inch-thick shells with the 2.0- and 3.0-inch-long cracks experience a change in the local buckling mode. The filled symbols in Figs. 4-7 identify the loads that correspond to secondary buckling, or the change in the local buckling mode near the crack. The initial postbuckling response of the shells is unstable after the mode change, and as a result, the axial load decreases after buckling occurs. The magnitude of the load decrease, the postbuckling deformation pattern and the overall axial postbuckling stiffness of the shell is dependent on the material behavior, as described subsequently. The unstable transition region in the response predictions is indicated by the broken lines in Figs. 4a-7a. The unstable transition from the stable initial buckled configuration to the stable postbuckling configuration was determined by using the transient analysis capability in STAGS. The transient analysis was continued until the kinetic energy in the system was negligible. Once a stable equilibrium state was determined from the transient analysis, the nonlinear static analysis was resumed to compute the stable postbuckling equilibrium response results shown in Figs 4a-7a. The stable postbuckling segments in the response curves are accompanied by an increase in the magnitude of the local

4
American Institute of Aeronautics and Astronautics

deformations in the shell near the crack. In addition, the slope of the postbuckling stable equilibrium segment of the response curve decreases as loading continues in the postbuckling range, indicating a reduction in the effective axial compressive stiffness of the shell. This reduction in stiffness is due to increasing deformations in the vicinity of the crack as the compression load is increased, which results in significant load redistribution in the shell away from the crack. The overall collapse of the 0.040-inch-thick shells with the 3.0- and 4.0-inch-long cracks and the 0.020-inch-thick shells with the 2.0- and 3.0-inch-long cracks occurs at the **X** on the associated curve. The unstable collapse response is represented by the dotted lines in the figures and is characterized by a significant reduction in the axial compression load and the development of the general instability mode in the shell.

The initial local buckling load, secondary buckling load, and shell collapse load predictions obtained from elastic and elastic-plastic analyses for the 0.040- and 0.020-inch-thick shells are summarized in Fig. 8, and in Tables 1 and 2, respectively. Buckling load predictions for an undamaged shell are also provided in Fig. 8. These results indicate that the magnitudes of the initial buckling loads and secondary buckling loads decrease as the initial crack length increases. Furthermore, the initial buckling load and secondary buckling load predictions obtained from the elastic and the elastic-plastic analyses are basically the same. For the 0.040-inch-thick shells, with 2.0-, 3.0-, and 4.0-inch-long cracks, local yielding occurs at the crack center and at the crack tips after initial buckling and as the radial displacements become large. However, the yielding is extremely localized and does not affect the secondary buckling load. For the 0.020-inch-thick shells, yielding does not occur until after the change in the local buckling mode. Consequently, as shown in Fig. 9, the initial local buckling load results and the secondary local buckling load results obtained from an elastic and an elastic-plastic analysis for the 0.020-

and 0.040-inch-thick shells are represented very well by a characteristic curve that is based on the curvature parameter $a/\sqrt{Rt}$.

The collapse load predictions, however, are not represented by a characteristic curve that is based on the curvature parameter $a/\sqrt{Rt}$. Collapse load predictions obtained from both an elastic analysis and an elastic-plastic analysis for the 0.020-inch-thick shell indicate that, although the initial and secondary buckling loads for the 0.020-inch-thick shell with a 2.0-inch-long crack are larger than the corresponding buckling loads for the shell with a 3.0-inch-long crack, the collapse load is smaller. This behavior is a consequence of the initial postbuckling deformations in the 0.020-inch-thick shell with a 2.0-inch-long crack extending circumferentially over a larger portion of the shell than the initial postbuckling deformations in the shell with a 3.0-inch-long crack. The initial postbuckling deformations from an elastic-plastic analysis of a 0.020-inch-thick shell with a 2.0-inch-long and a 3.0-inch-long crack are provided in Fig. 10. Predictions obtained from an elastic analysis were basically the same. The more extensive deformations in the shell with a 2.0-inch-long crack results in significant stress redistribution away from the crack, and a larger reduction in the effective postbuckling axial stiffness of the shell with the 2.0-inch-long crack, as indicated by the reduction in the slope of the postbuckling portion of the response curves shown in Figs. 6 and 7. In addition, comparison of the predictions from an elastic and an elastic-plastic analysis for the compression response of the 0.020-inch-thick shells with 2.0- and 3.0-inch-long cracks, and the 0.040-inch-thick shells with 3.0- and 4.0-inch-long cracks indicates that the collapse loads predicted by an elastic-plastic analysis are greater than those predicted by an elastic analysis. Furthermore, the results from the elastic-plastic analysis indicate that for the 0.040-inch-thick shells with 3.0-, and 4.0-inch-long cracks the decrease in load associated with the unstable local buckling event that occurs near the crack is

Table 1. Buckling load predictions for a 0.040-inch-thick shell

Crack Length, 2a (in.)	$a/\sqrt{Rt}$	Initial Buckling P/P_{cr}		Secondary Buckling P/P_{cr}		Collapse P/P_{cr}	
		Elastic	Elastic-Plastic	Elastic	Elastic-Plastic	Elastic	Elastic-Plastic
1.0	0.833	0.819	0.819	0.854	0.853	0.854	0.853
2.0	1.667	0.530	0.530	0.575	0.573	0.575	0.573
3.0	2.500	0.389	0.365	0.476	0.471	0.503	0.589
4.0	3.333	0.313	0.306	0.422	0.422	0.501	0.579

Table 2. Buckling load predictions for a 0.020-inch-thick shell

Crack Length, 2a (in.)	$a/\sqrt{Rt}$	Initial Buckling P/P_{cr}		Secondary Buckling P/P_{cr}		Collapse P/P_{cr}	
		Elastic	Elastic-Plastic	Elastic	Elastic-Plastic	Elastic	Elastic-Plastic
1.0	1.178	0.731	0.731	0.735	0.735	0.735	0.735
2.0	2.357	0.407	0.407	0.484	0.484	0.419	0.438
3.0	3.535	0.301	0.301	0.406	0.406	0.532	0.566

smaller than that obtained from the elastic analysis, and a larger postbuckling stiffness is predicted by the elastic-plastic analysis.

Typical results of the load-shortening predictions, deformation pattern predictions, and stress resultant predictions obtained from a linear elastic and an elastic-plastic analysis for the 0.040-inch-thick shell with a 3.0-inch-long crack are shown in Figs. 11-14 to illustrate the differences in the material linear and material nonlinear analysis predictions. The load-shortening response curves from an elastic and an elastic-plastic analysis are given in Fig. 11a and provide an overall comparison of the compression response predictions from the two analyses. The load-time history of the unstable local buckling response is shown in Fig. 11b. Initial yielding occurs for an applied load corresponding to $P/P_{cr} =$ 0.43, which is approximately 90 percent of the buckling load associated with the local mode change. Deformed shapes obtained from an elastic analysis and an elastic-plastic analysis are provided in Figs. 12 and 13, respectively, to show the development of the shell's postbuckling response. The deformed shapes in Figs. 12 and 13 correspond to the points A, B, C, and D on the load-shortening curves shown in Fig. 11.

The load-shortening predictions based on an elastic analysis and an elastic-plastic analysis, and the deformation pattern prediction at point A, just prior to the local mode change, indicate that the shell response prior to the local mode change is adequately predicted by an elastic analysis. The initial buckling deformation pattern, shown as deformation pattern A in Figs. 12 and 13, is typical of the shape of the initial buckling deformation pattern for the 0.040-inch-thick shell with the 2.0-, 3.0- and 4.0-inch-long cracks, and for the 0.020-inch-thick shell with the 2.0-, and 3.0-inch-long cracks. The initial buckling deformation is characterized by inward buckles at the crack tips, and outward deformations along the crack edges. As the postbuckling response progresses from point A to point B, the buckle pattern rotates around the radial coordinate axis. In the elastic case, the buckle rotates 90 degrees around the radial coordinate axis, re-

sulting in a deformation pattern with high circumferential curvature, that apparently stiffens the skin longitudinally near the crack enough to stabilize the shell and to increase the amount of axial compression load that can be supported by the shell after the local mode change occurs. The initial postbuckling pattern obtained from the elastic-plastic analysis, however, is significantly different, as shown in Fig. 13 (deformation pattern B). The initial postbuckling deformation pattern predicted by the elastic-plastic analysis is very similar to the deformation pattern labeled A* in Fig. 12 and predicted by the elastic, transient analysis. These results suggest that for the shell studied, yielding of the aluminum prevents the postbuckling deformation pattern, B, predicted by the elastic analysis from developing. This result is consistent with the experimentally observed response.[6]

As shown in Fig. 11, the elastic-plastic analysis predicts a less severe decrease in the load associated with the unstable local buckling event that occurs near crack than is predicted by the elastic analysis. Furthermore, the elastic-plastic analysis predicts greater axial postbuckling stiffness than is predicted by the elastic analysis. This behavior is a result of the local yielding near the crack, caused by large bending deformations, that effectively constrains the initial buckling pattern from rotating as far around the radial coordinate as predicted by the elastic analysis. As a consequence, a smaller portion of the shell is disturbed by the postbuckling deformations. In addition, the magnitude of the collapse load predicted by the elastic-plastic analysis is larger than the magnitude predicted by the elastic analysis. This difference is explained by comparing predictions from the elastic and elastic-plastic analyses for the axial and circumferential stress resultants just before shell collapse occurs. Contour plots of the axial and circumferential stress resultants corresponding to point C on the load shortening curves in Fig. 11, are provided in Fig. 14. Stress resultant distributions obtained from an elastic analysis and an elastic-plastic analysis are shown in Figs. 14a and 14b, respectively. These results indicate that the local postbuckling deformations have a significant influence on

the load distribution in the shell. In addition, the results indicate that regions of large destabilizing in-plane biaxial compression stress resultants develop near the crack, particularly in the elastic case. In the elastic case, the shell deformations with large circumferential curvature induce large circumferential compressive stresses, and result in the formation of longitudinal 'stiffener like' regions which support large amounts of axial compression load. In the elastic-plastic case, yielding in the vicinity of the local postbuckling deformations causes load to be redistributed to the opposite side of the shell, as shown in Fig. 14c, and the biaxial compression state near the crack is not as severe as for the elastic case. Consequently, the elastic-plastic shell can support more load before collapsing. However, as shown in Fig. 14c, the axial compression and circumferential compression stresses near the crack required to cause the shell to collapse are lower for the elastic-plastic case than they are for the elastic case, due to a 'softening' of the material behavior in the plastic region near the crack.

A similar comparison of the elastic and elastic-plastic response predictions for the 0.020-inch-thick shell with a 3.0-inch-long is provided in Figs. 15-17. The load-shortening response curves from an elastic and an elastic-plastic analysis are given in Fig. 15 as an overall comparison of the compression response predictions from the two analyses. An extensive postbuckling response is indicated by several stable and unstable segments in the load-shortening response curve. Unstable response segments are indicated by dotted lines. These results indicate that the shell response prior to the local mode change, and the shell response throughout the majority of the postbuckling range, is adequately predicted by an elastic analysis. For these thin shells, yielding does not start until after the local mode change and is very localized, developing only at the crack-tips and crack edges, and at the nodes in the deformed shell where the axial compression and circumferential stresses are large. The effect of plastic deformations on the overall response of these shells is therefore not as significant as for the 0.040-inch-thick shells.

The initial postbuckling deformation pattern predicted at point **B** on the load-shortening response curves by both an elastic and an elastic-plastic analysis is shown in Fig. 10b. As the load is increased further into the postbuckling response range, the deformation pattern gradually moves around the circumference of the shell, developing into patterns similar to those shown by points **C** and **D** in Fig. 12 for the elastic 0.040-inch-thick shell. For the 0.020-inch-thick shell, the circumferential half-wave length is shorter than for the 0.040-inch-thick shells. The shell is able to support significant load after initial postbuckling because the shell deformations with large circumferential curvature and regions of large outward radial deformations, introduce 'stiffener like' regions in the shell that support large amounts of axial compression load. This response behavior is demonstrated in Fig. 16 which shows the circumferential variation of the radial displacement and axial stress resultant at the shell midlength at selected points in the elastic-plastic response predictions. Curves in Fig. 16 designated **A**, **B**, **F**, and **J** correspond to points on the load-shortening curve in Fig. 15. Large axial stresses develop along the outward ridges in the deformed shell, and increase as the applied axial compression load increases. An indication of the effect of plasticity on the destabilizing biaxial in-plane compression resultants that develop in the deformed shell is provided in Fig. 17. Point **I** corresponds to the response just before predicted collapse by the elastic analysis, and Point **J** corresponds to the response just before predicted collapse by the elastic-plastic analysis. For the elastic-plastic case, yielding in the vicinity of the local postbuckling deformations causes the destabilizing biaxial compression state to be less severe than for the elastic case. Consequently, the elastic-plastic shell can support more load before collapsing than can the elastic shell.

Internal Pressure and Axial Compression Loads - No Crack Extension

A summary of the effects of combined internal pressure and axial compression loads on the initial buckling load and collapse load for a 0.040-inch-thick shell with initial crack lengths of 2.0, 3.0 and 4.0 inches is shown in Fig. 18a and Fig. 18b, respectively for 0, 10, 30, and 50 psi of internal pressure. Predictions based on both an elastic analysis and an elastic-plastic analysis are provided. The results in Fig. 18a indicate that the initial buckling load of the shells increases as the internal pressure increases for a given crack length. The initial buckling load increases because of the larger tensile circumferential stress resultants near the crack for larger magnitudes of internal pressure, which tend to stabilize the shell. Results of the elastic-plastic analysis, however, show a less significant increase in the buckling load with increase in pressure, particularly at higher magnitudes of internal pressure and for shells with shorter crack lengths, where higher axial stresses are required to cause buckling of the shell to occur. These results indicate that the buckling load predictions from an elastic analysis may be unconservative. The results also indicate that the buckling load decreases as the crack length increases for a given value of internal pressure. The results in Fig. 18b indicate that the collapse load of the shells, in general, increases as the internal pressure increases for a given crack length, and that the increase predicted by an elastic analysis is larger than the increase predicted by an elastic-plastic analysis. In addition, the

elastic-plastic analysis predicts a lower collapse load for 30 psi of internal pressure than for 10 and 50 psi of internal pressure.

Results for a 0.040-inch-thick shell with a 3.0-inch-long crack are presented in Figs. 19 and 20 to demonstrate typical response characteristics of a shell with a crack and subjected to combined internal pressure and axial compression loads. The load-shortening response curve in Fig. 19 provides an overall guide to the response. The results indicate that the magnitude of the first local buckling load of the shells increases as the internal pressure level increases. For the combined load case, the first local buckling mode corresponds to a change in the shell deformation from a symmetric local pattern to an unsymmetric local pattern, and not to growth of the symmetric local pattern as for the axial compression load case. In addition, the results indicate that for low values of internal pressure, the initial postbuckling response is unstable, and that the initial local postbuckling response transitions to a stable postbuckling response as the internal pressure level increases. For the results presented in Fig. 19, shells with an internal pressure level equal to or greater than 30 psi exhibit a stable local postbuckling response. The results also show that the general instability load for the shells increases with increases in internal pressure, and that the amount of reduction in load associated with collapse decreases as the internal pressure level increases.

Representative initial postbuckling and general instability deformed shape plots are provided in Fig. 20 for a shell with a 3.0-inch-long crack and subjected to 30 psi of internal pressure. The local crack prebuckling deformation pattern is similar to that shown in Fig. 13 (point A), for the axial compression case, but it has significantly larger deformations. Furthermore, for the cases considered here, the prebuckling deformation pattern is always symmetrical with respect to the planes $x = 0$ and $\theta = 0°$. Therefore, the crack behavior in the prebuckled state can be characterized by the Mode I crack-opening fracture mode. The stable postbuckling deformation shape, after the local mode change, is shown in Fig. 20a. The deformation pattern in Fig. 20a indicates that the shell deforms into an unsymmetric local pattern with high circumferential curvature gradients at the crack tips. The crack behavior in the postbuckling state therefore cannot be characterized by a simple Mode I crack-opening response. Consequently, only the interaction between crack extension and initial local buckling is addressed in the next section. The general instability deformation pattern, shown in Fig. 20b, indicates that an increase in internal pressure results in a deformation with a shorter circumferential half-wave length than for the unpressurized case.

Internal Pressure and Axial Compression Loads - Crack Extension

Results are presented in Fig. 21 for a 0.040-inch-thick shell with a 3.0-inch-long initial crack to provide a preliminary indication of the effect of crack growth on the initial buckling load. Crack growth was simulated using the critical CTOA criterion, and a critical angle equal to 5.36°. The results shown in Fig. 21 were generated from an elastic-plastic analysis by first applying a live internal pressure load of the desired load level to the shell. After this load level was attained, an increasing axial compression load was applied. The effect of load sequence on the results was not investigated. The bottom curve in the figure corresponds to the combination of internal pressure and axial compression loads required to initiate stable crack growth. For this shell, crack propagation initiates for internal pressure only, at an internal pressure level of 30 psi. The top curve indicates the effect of internal pressure on the initial buckling load for a shell with a fixed crack length. The dashed curve shows the effect of crack growth on the initial buckling load. These results show that for the shell considered, and for internal pressure load magnitudes less than 30 psi, crack growth reduces the buckling load by 10% or less. For larger magnitudes of internal pressure, the effect of crack growth on the initial buckling load is expected to be more significant. Crack growth for internal pressure loads greater than 30 psi extends to the boundaries of the refined mesh shown in Fig. 3b, and the interaction between crack growth and initial buckling could not be evaluated with this model.

Concluding Remarks

The results of an analytical study of the effects of a longitudinal crack on the nonlinear response of thin unstiffened aluminum cylindrical shells subjected to axial compression, and to combined internal pressure and axial compression loads are presented. The results indicate that the nonlinear interaction between the in-plane stress resultants and the out-of-plane displacements near a crack in a thin shell can significantly affect the structural response of the shell. Large local stress and displacement gradients exist near a crack in a shell for all loading conditions considered in the present study. The results indicate that the nonlinear response of the shell depends on the loading condition applied to the shell and the initial crack length. The initial buckling load of a shell subjected to axial compression loads decreases as the initial crack length increases. Initial buckling causes general instability or collapse of the shell for shorter initial crack lengths. Initial buckling is a stable local response for longer initial crack lengths. This stable local buckling response is followed by a stable postbuckling response, which is followed by general or overall instability of the

shell. The results for combined internal pressure and axial compression loads indicate that the initial buckling load of a shell increases as the magnitude of the internal pressure increases, but decreases as the inital crack length increases. Furthermore, results indicate that predictions from an elastic analysis for the initial buckling load of a cracked shell subjected to combined axial compression and internal pressure can be unconservative.

References

[1]Riks, E., "Bulging Cracks in Pressurized Fuselages: A Numerical Study," NLR MP 87058 U, NLR National Aerospace Laboratory, The Netherlands, September 1987.

[2]Rankin, C. C., Brogan, F. A., and Riks, E., "Some Computational Tools for the Analysis of Through Cracks in Stiffened Fuselage Shells," *Computational Mechanics*, Springer International, Vol. 13, No. 3, December 1993, pp. 143-156.

[3]Starnes, J. H., Jr., Britt, V. O., and Rankin, C. C., "Nonlinear Response of Damaged Stiffened Shells Subjected to Combined Internal Pressure and Mechanical Loads," AIAA Paper 95-1462, April 1995.

[4]Starnes, J. H., Jr., Britt, V. O., Rose, C. A., and Rankin, C., C., "Nonlinear Response and Residual Strength of Damaged Stiffened Shells Subjected to Combined Loads," AIAA Paper No. 96-1555, April 1995.

[5]Starnes, J. H., Jr., and Rose, C. A., "Nonlinear Response of Thin Cylindrical Shells with Longitudinal Cracks and Subjected to Internal Pressure and Axial Compression Loads," AIAA Paper No. 97-1144, April, 1997.

[6]Starnes, J. H., Jr., and Rose, C. A., "Buckling and Stable Tearing Responses of Unstiffened Aluminum Shells with Long Cracks," AIAA Paper No. 98-1191, April 1998.

[7]Estekanchi, H. E., and Vafai, A., "On the Buckling of Cylindrical Shells with Through Cracks Under Axial Load," *Thin-Walled Structures*, Vol. 35, 1999, pp. 255-274.

[8]Dawicke, D. S., Sutton, M. A., Newman, J. C., Jr., and Bigelow, C. A., "Measurement and Analysis of Critical CTOA for Aluminum Allow Sheet," NASA TM-109024, September, 1993.

[9]Brogan, F. A., Rankin, C. C., and Cabiness, H. D., "STAGS User Manual," Lockheed Palo Alto Research Laboratory, Report LMSC P032594, 1994.

[10]Riks, E., "Some Computational Aspects of the Stability Analysis of Nonlinear Structures," *Computational Methods in Applied Mechanics and Engineering*, Vol. 47, 1984, pp. 219-259.

[11]Riks, E., "Progress in Collapse Analysis," *Journal of Pressure Vessel Technology*, Vol. 109, 1987, pp. 27-41.

[12]Riks, E., Rankin, C. C., and Brogan, F. A., "On the Solution of Mode Jumping Phenomena in Thin-Walled Shell Structures," *Computational Methods in Applied Mechanics and Engineering*, September 1996, pp. 59-92.

[13]Park, K. C., "An Improved Stiffly Stable Method for Direct Integration of Nonlinear Structural Dynamics," *Journal of Applied Mechanics*, Vol. 42, June 1975, pp. 464-470.

[14]Riks, E., Brogan, F. A., and Rankin, C. C., "Bulging of Cracks in Pressurized Fuselages: A Procedure for Computation," in Analytical and Computational Models of Shells, Noor, A. K., Belytschko, T., and Simo, J. C., Editors, The American Society of Mechanical Engineers, ASME-CED Vol. 3, 1989.

[15]Newman, J. C., Jr., "An Elastic-Plastic Finite Element Analysis of Crack Initiation, Stable Crack Growth and Instability," ASTM STP 833, 1984, pp. 93-117.

[16]Rankin, C. C., and Brogan, F. A., "The Computational Structural Mechanics Testbed Structural Element Processor ES5: STAGS Shell Element," NASA Contractor Report 4358, May 1991.

[17]Besseling, J. F., "A Theory of Elastic, Plastic and Creep Deformations on an Initially Isotropic Material Showing Anisotropic Strain-Hardening, Creep Recovery, and Secondary Creep," *ASME Journal of Applied Mechanics*, 1958, pp. 529-536.

[18]Zienkiewicz, O. C., Nayak, G. C. and Owen, D. R. J., "Composite and 'Overlay' Models in Numerical Analysis of Elasto-Plastic Continua," Foundations of Plasticity, A. Sawczok Ed. Nordhoff Press, pp. 107-122, 1972.
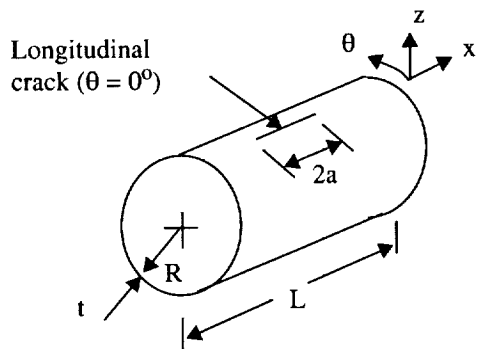
Figure 1. Shell geometry.
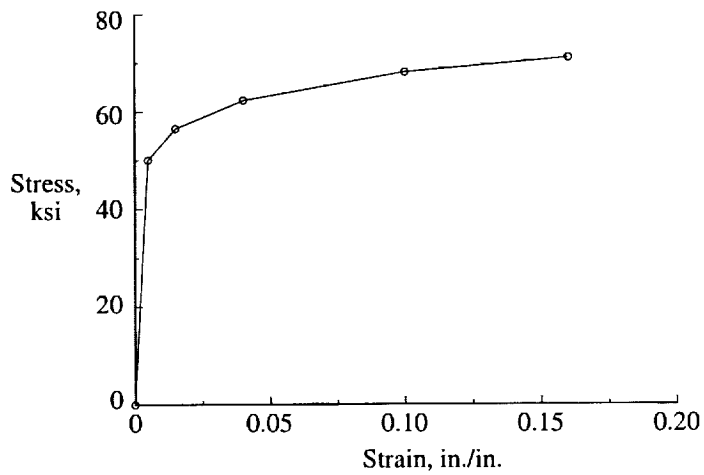
Stress (ksi)	Strain (in./in.)
0.00	0.00
50.0	0.0048
56.6	0.015
62.3	0.040
68.2	0.100
71.1	0.160

E = 10.35 Msi
v = 0.3

Figure 2. Piecewise linear representation for the uniaxial stress-strain curve for 2024-T3 aluminum (L-T orientation).
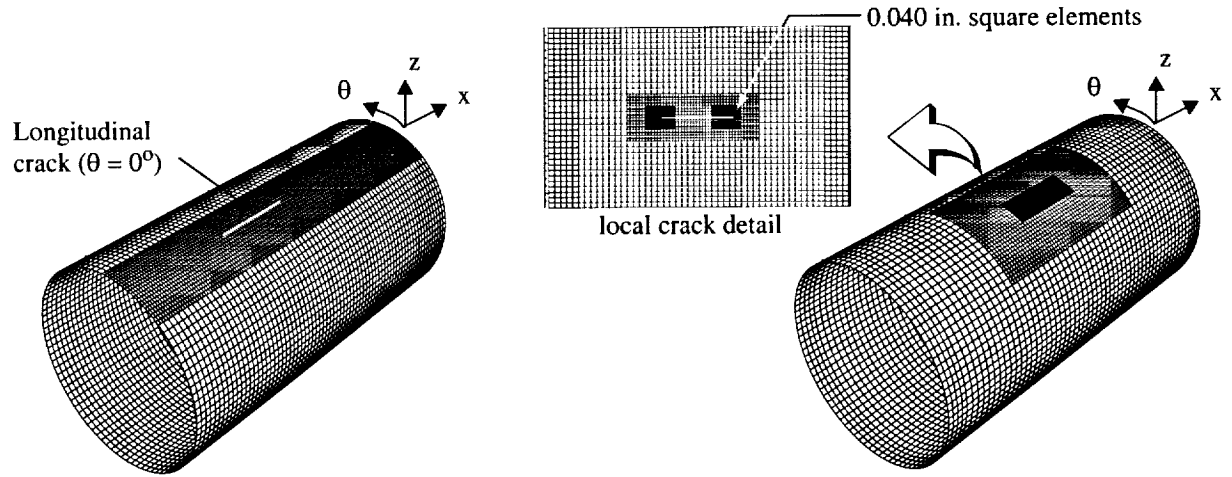
(a) Finite element model for axial compression and combined internal pressure and axial compression loads, without crack extension

(b) Finite element model for combined internal pressure and axial compression loads with crack extension

Figure 3. Finite element models for axial compression and combined internal pressure and axial compression loading cases.

(a) Load-shortening response

(b) Load-normal displacement response
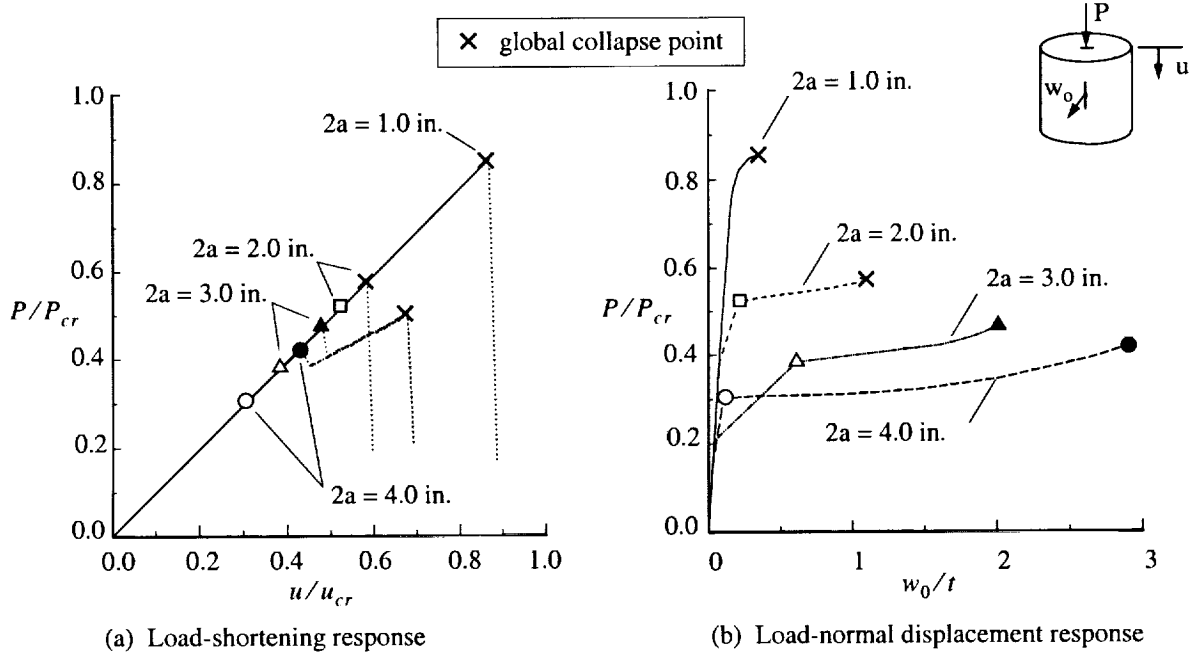
Figure 4. Effect of longitudinal crack length on the linear-elastic response of 0.040-inch-thick cylindrical shells subjected to axial compression loads.
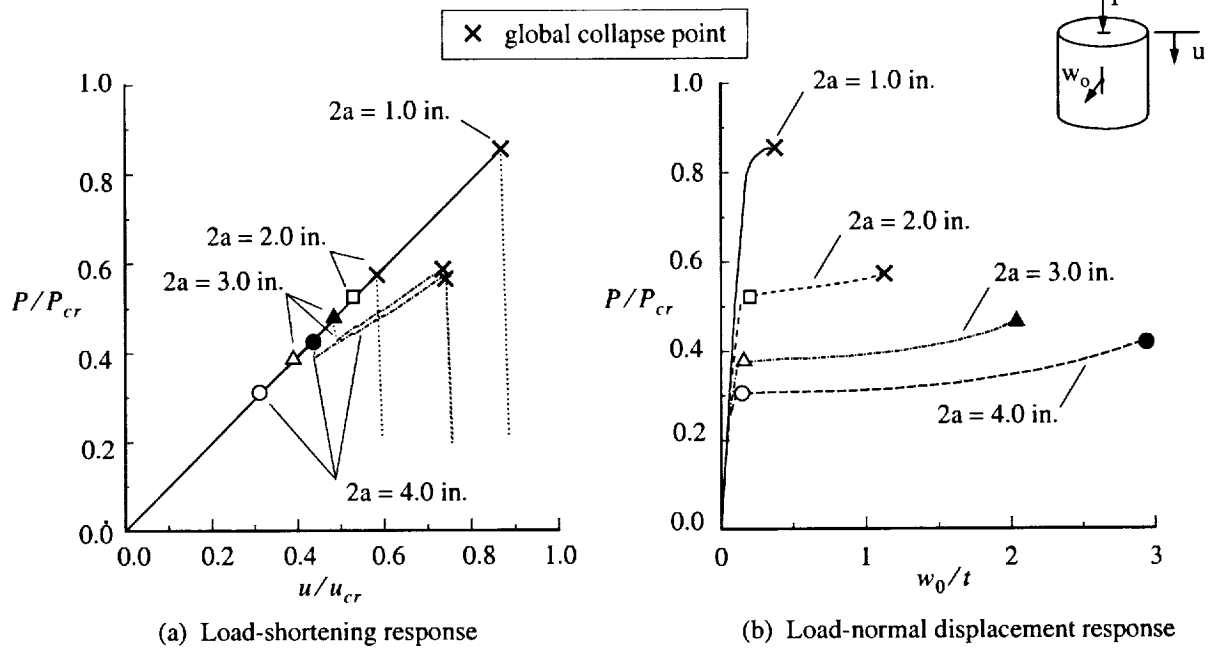
Figure 5. Effect of longitudinal crack length on the elastic-plastic response of 0.040-inch-thick cylindrical shells subjected to axial compression loads.

(a) Load-shortening response

(b) Load-normal displacement response

(a) Load-shortening response

(b) Load-normal displacement response
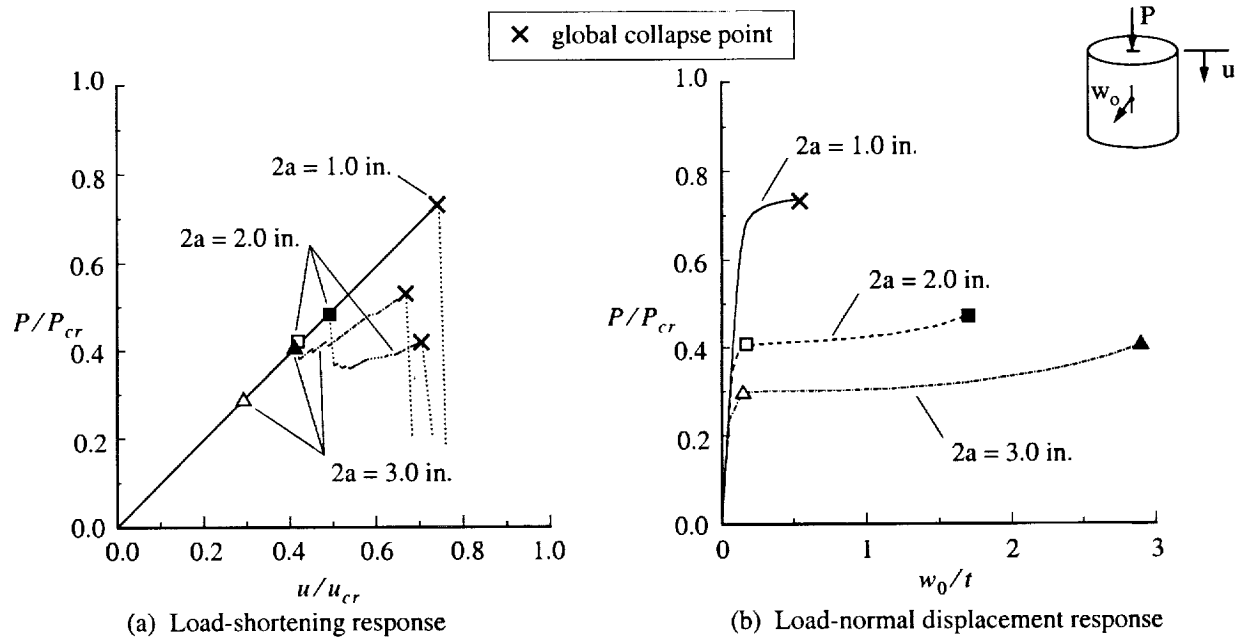
Figure 6. Effect of longitudinal crack length on the linear-elastic response of 0.020-inch-thick cylindrical shells subjected to axial compression loads.

12

American Institute of Aeronautics and Astronautics

(a) Load-shortening response

(b) Load-normal displacement response
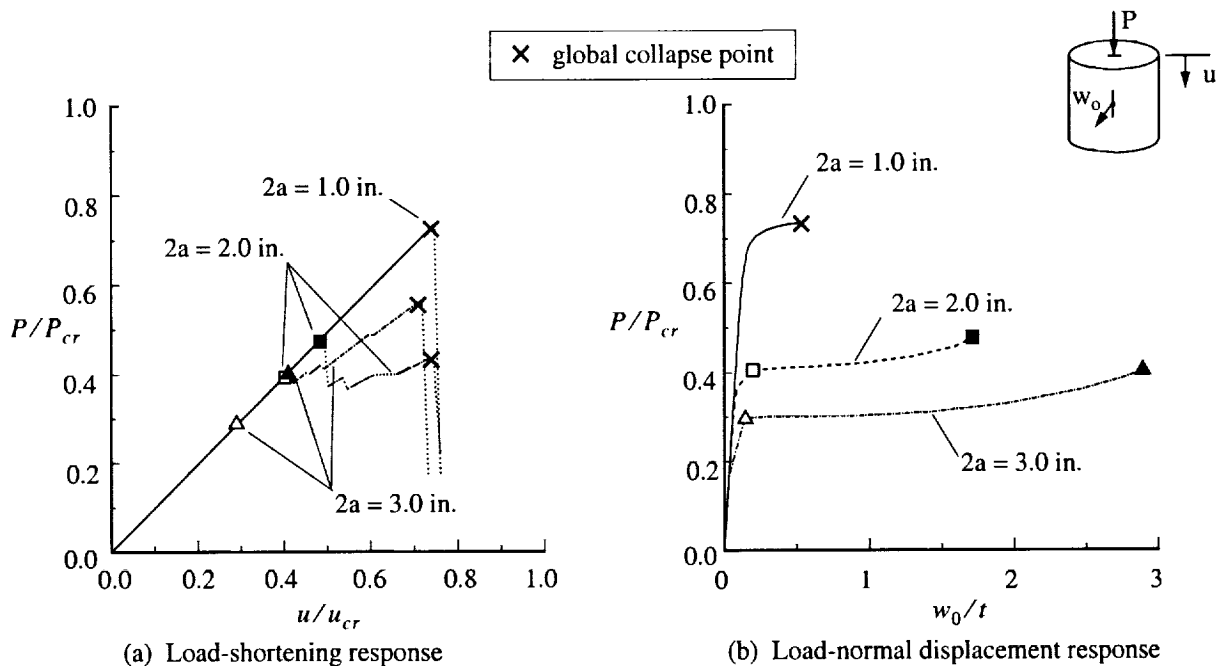
Figure 7. Effect of longitudinal crack length on the elastic-plastic response of 0.020-inch-thick cylindrical shells subjected to axial compression loads.
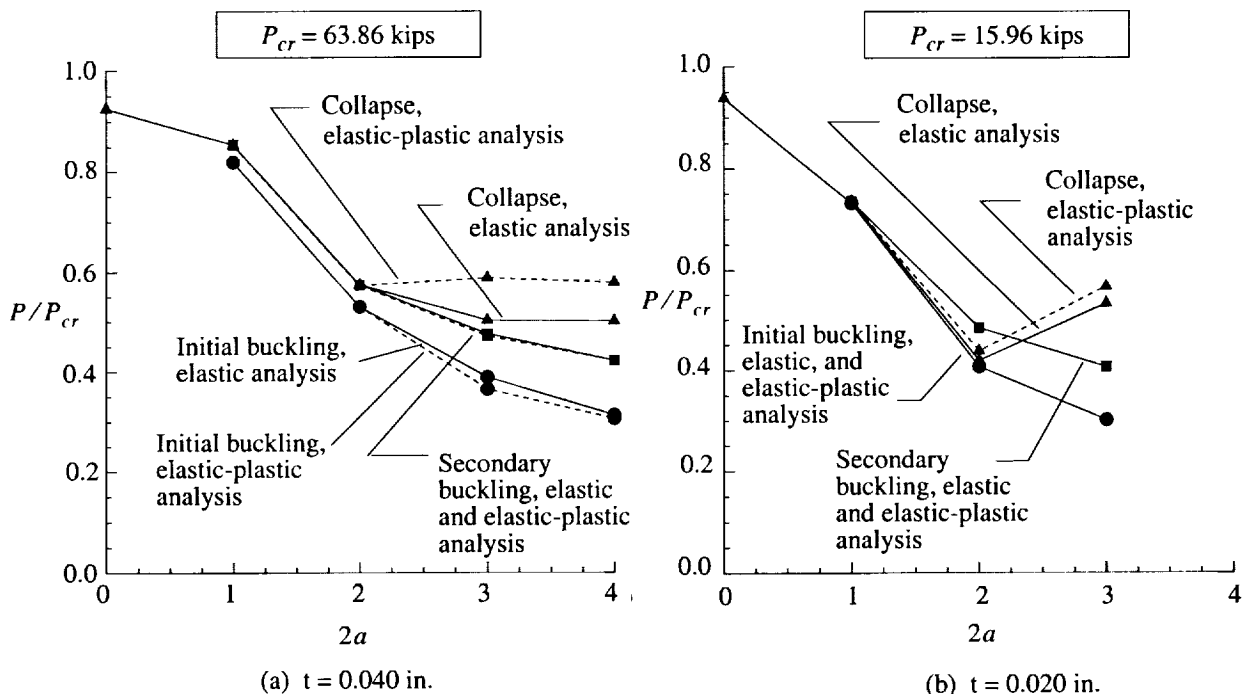
(a) t = 0.040 in.

(b) t = 0.020 in.

Figure 8. Buckling load as a function of the total crack length, for shells with thicknesses equal to 0.040 in. and 0.020 in.

(a) Initial and secondary buckling load

(b) Collapse load
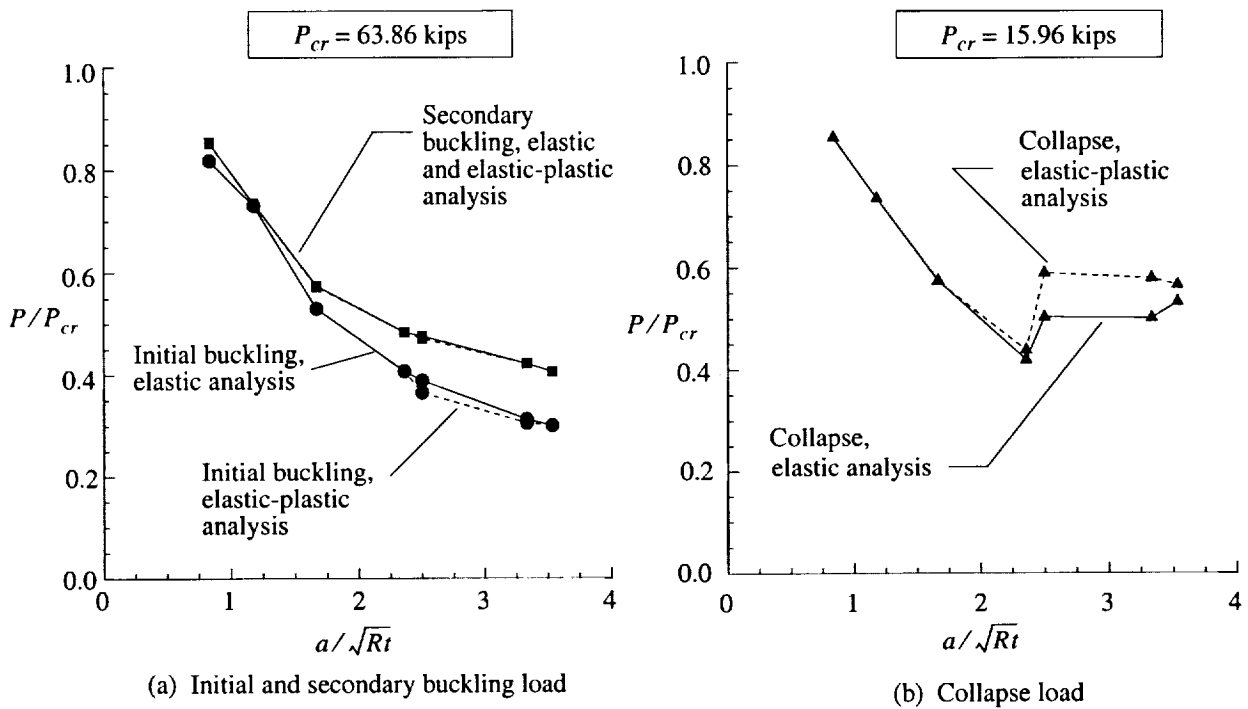
Figure 9. Buckling load as a function of the shell parameter, $a/\sqrt{Rt}$, for shells with thicknesses equal to 0.040 in. and 0.020 in.

(a) 2.0-inch-long longitudinal crack

(b) 3.0-inch-long longitudinal crack
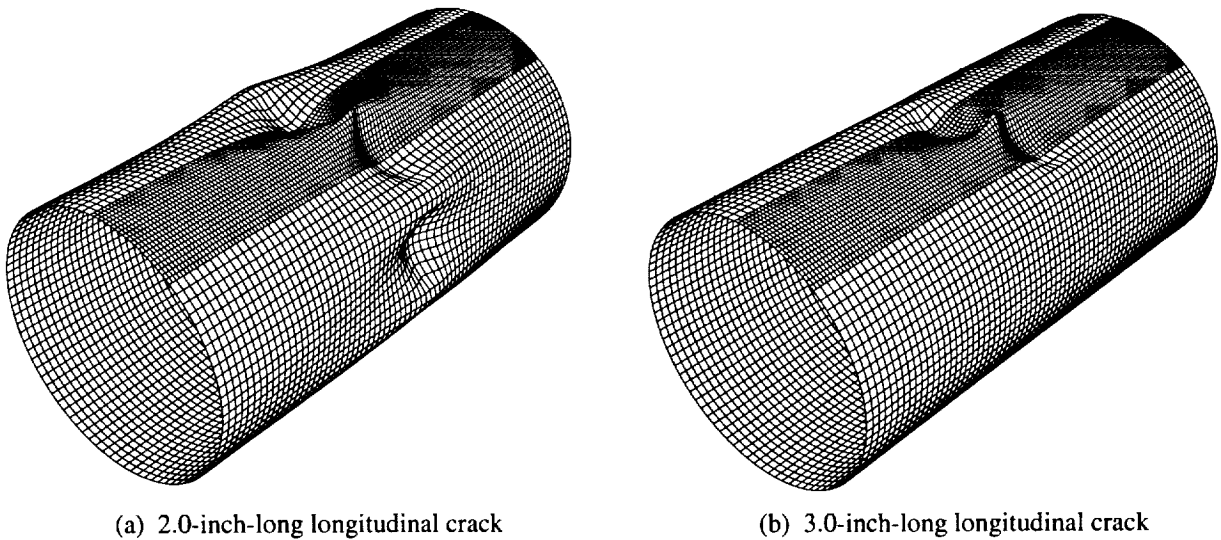
Figure 10. Comparison of initial postbuckling deformation patterns from an elastic-plastic analysis of a 0.020-inch-thick shell with a 2.0-inch-long and a 3.0-inch-long longitudinal crack and subjected to axial compression loads.

(a) Load-shortening response   (b) Load-time history response
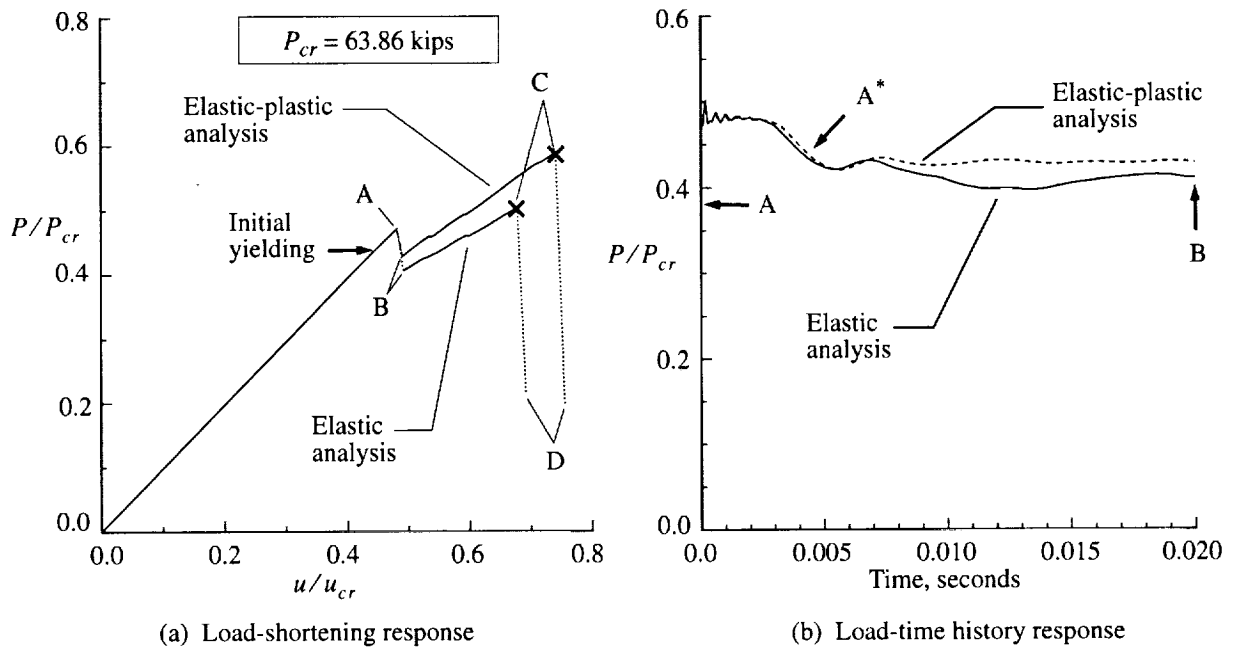
Figure 11. Comparison of load-shortening response predictions and load-time history of unstable local mode change obtained from an elastic analysis and an elastic-plastic analysis for a 0.040-inch-thick shell with a 3.0-inch-long longitudinal crack.

A   A*

B   C

D
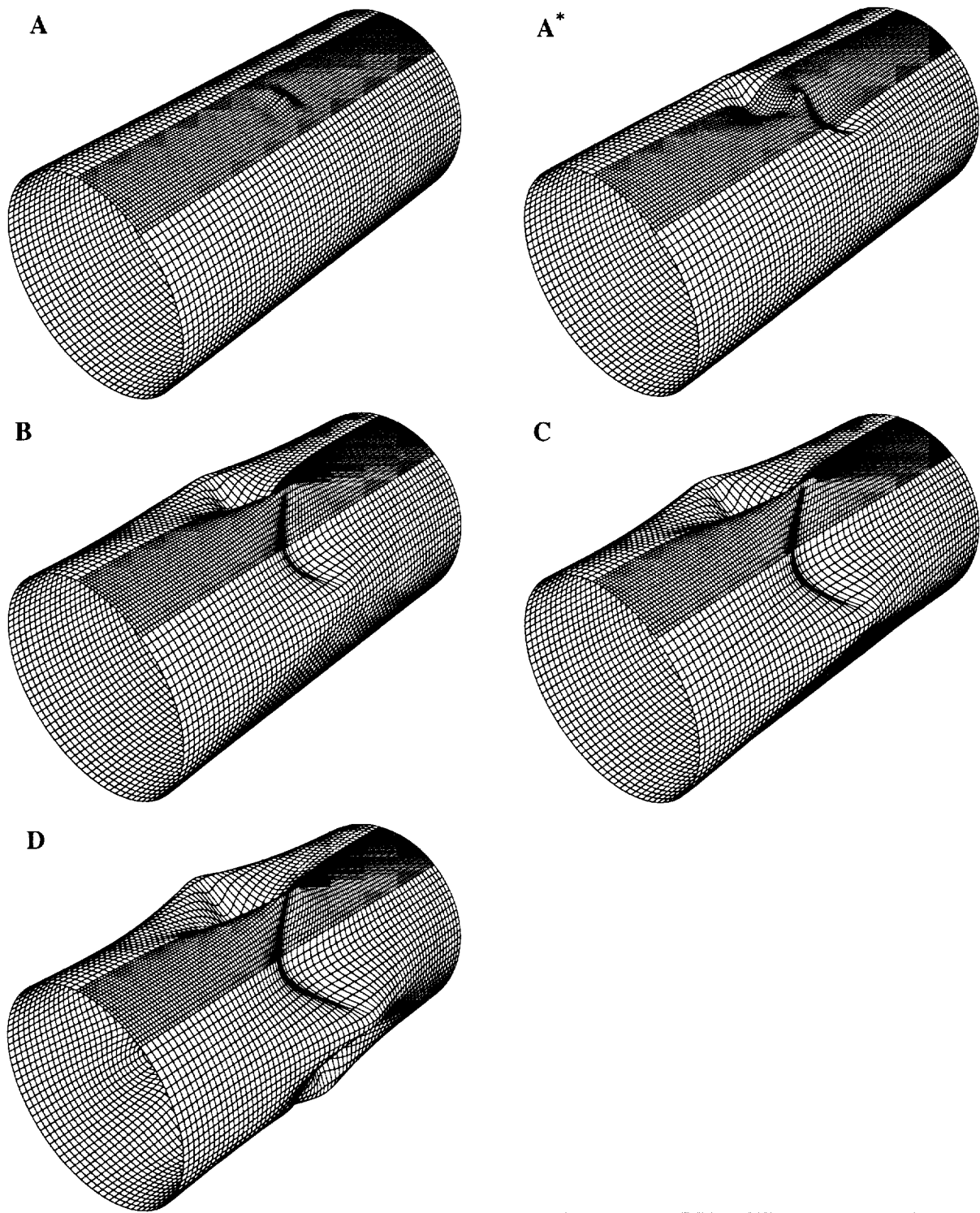
Figure 12. Selected deformation pattern predictions from an elastic analysis of a 0.040-inch-thick shell with a 3.0-inch-long longitudinal crack and subjected to axial compression loads (refer to Fig. 11 for selected points).
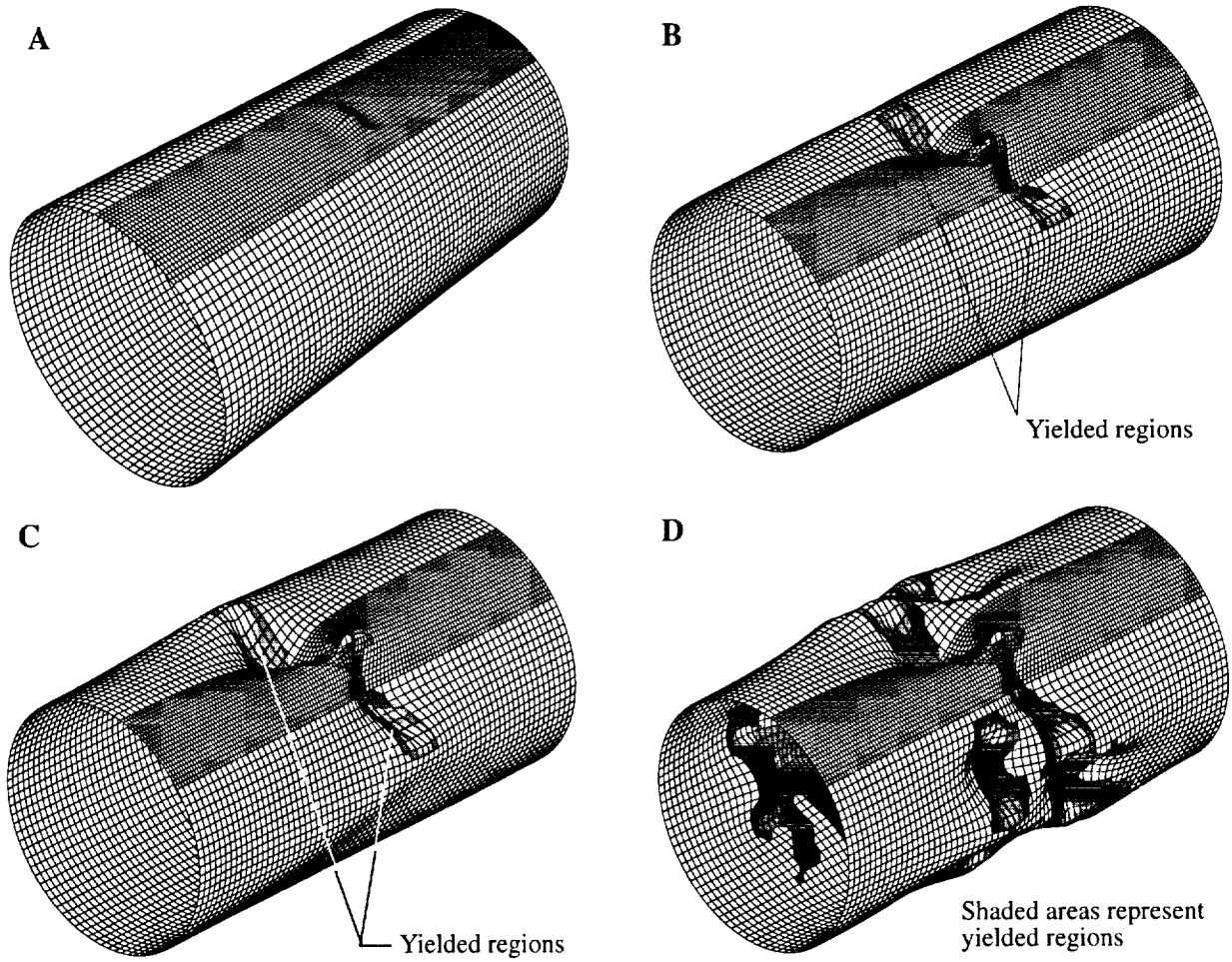
Figure 13. Selected deformation pattern predictions from an elastic-plastic analysis of a 0.040-inch-thick shell with a 3.0-inch-long longitudinal crack and subjected to axial compression loads (refer to Fig. 11 for selected points).
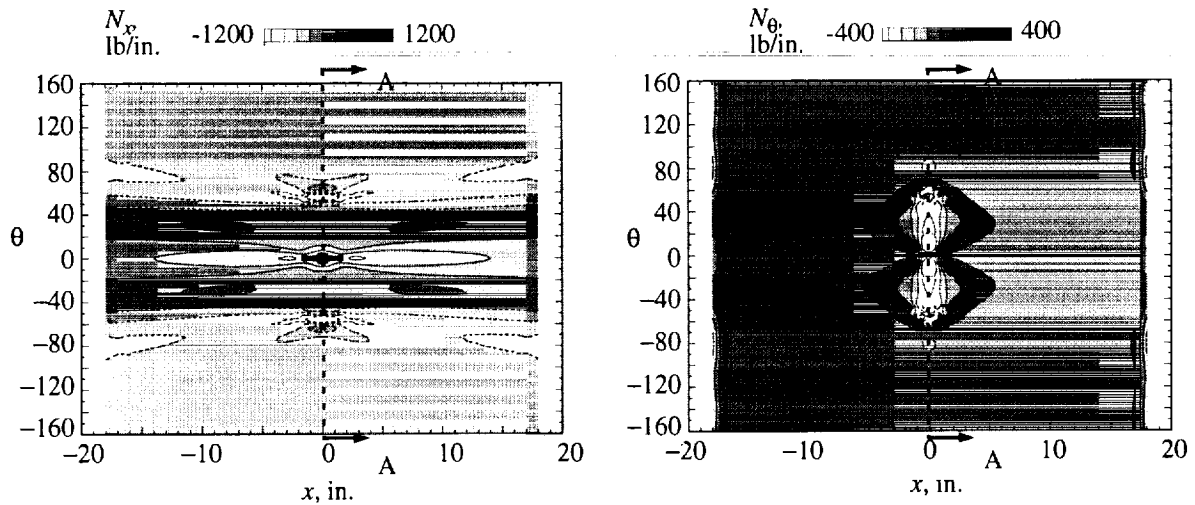
(a) Stress resultant distributions, just before collapse, elastic analysis
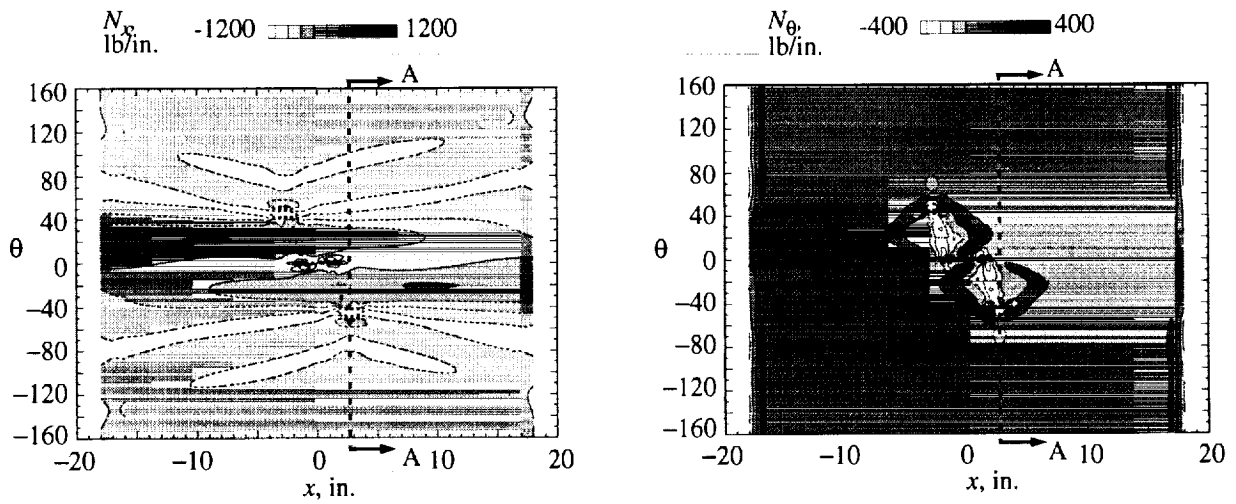
(b) Stress resultant distributions, just before collapse, elastic-plastic analysis
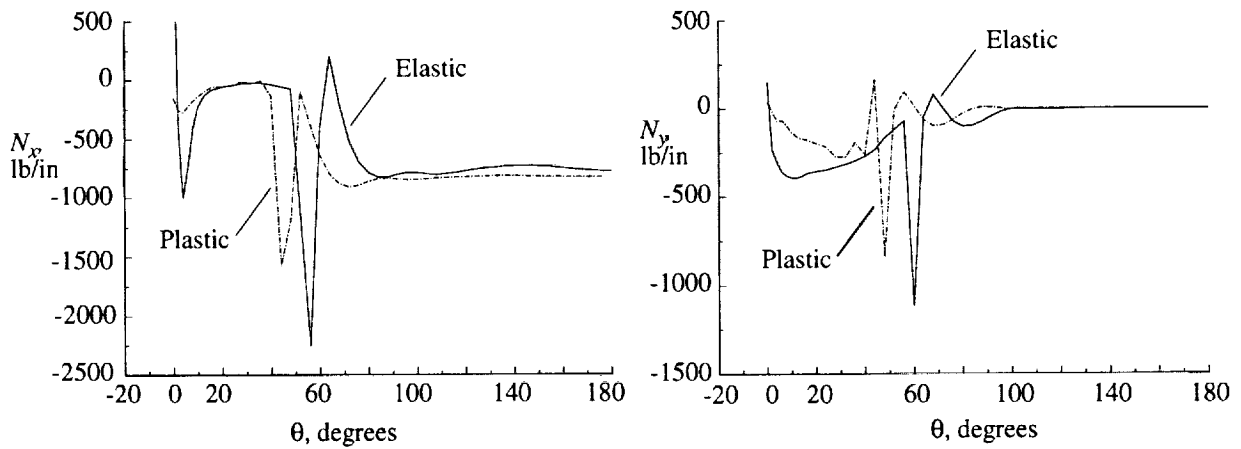
(c) Stress resultants along A-A, just before collapse, elastic analysis and elastic-plastic analysis

Figure 14. Comparison of stress resultant predictions from an elastic-plastic analysis and an elastic analysis of a 0.040-inch-thick shell with a 3.0-inch-long longitudinal crack and subjected to axial compression loads.
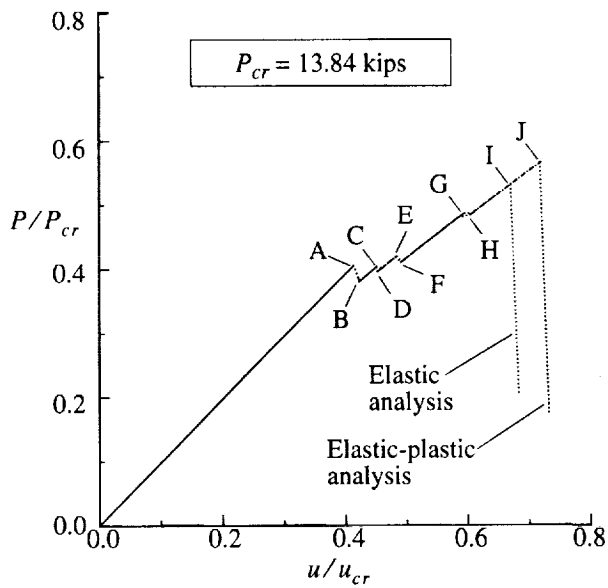
Figure 15. Comparison of load-shortening response predictions obtained from an elastic analysis and an elastic-plastic analysis of a 0.020-inch-thick shell with a 3.0-inch-long longitudinal crack and subjected to axial compression loads.


(a) Radial displacements

(b) Axial stress resultant
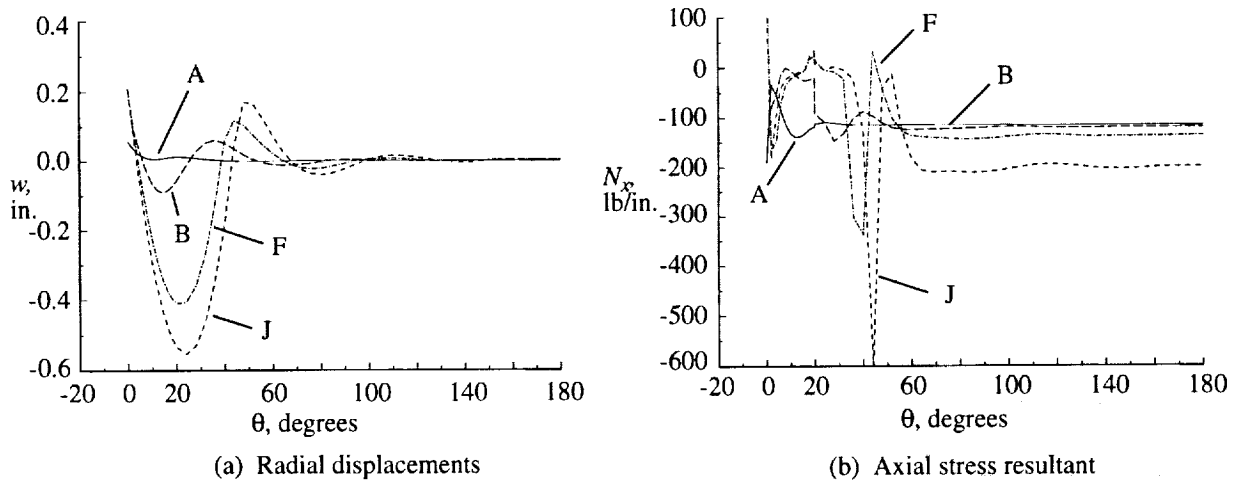
Figure 16. Radial displacements and axial stress resultants along $x = 0.0$ in. at selected points in the elastic-plastic response predictions for a compression-loaded 0.020-inch-thick shell with a 3.0-inch-long longitudinal crack (refer Fig. 15 for selected points).

20
American Institute of Aeronautics and Astronautics

(a) Axial stress resultant

(b) Circumferential stress resultant
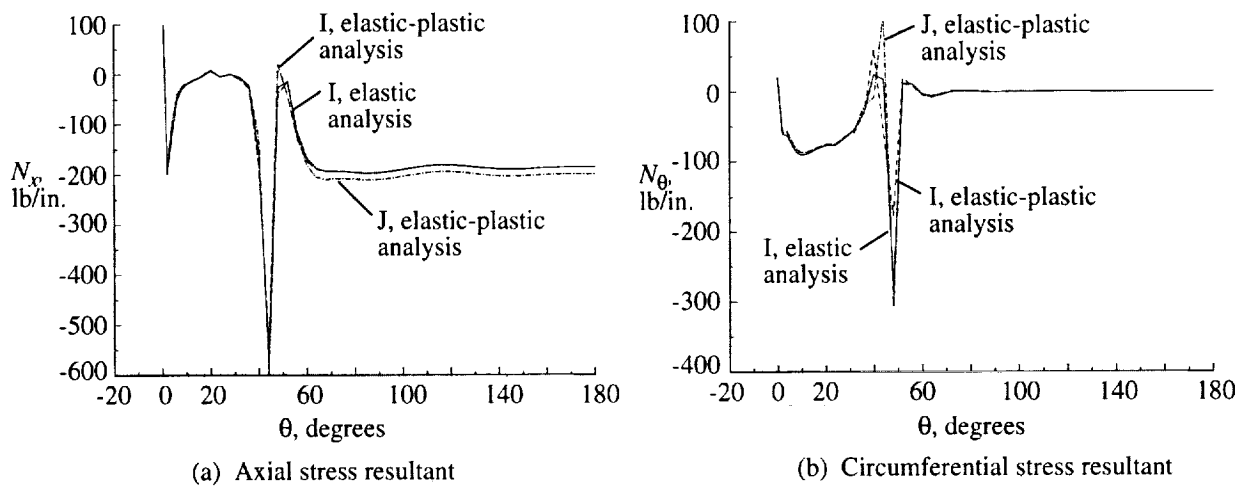
Figure 17. Comparison of axial stress resultants and circumferential stress resultants along $x = 0.0$ in., just prior to collapse, from an elastic analysis and an elastic-plastic analysis of a compression-loaded 0.020-inch-thick shell with a 3.0-inch-long longitudinal crack (refer to Fig. 15 for selected points).


(a) Initial buckling load
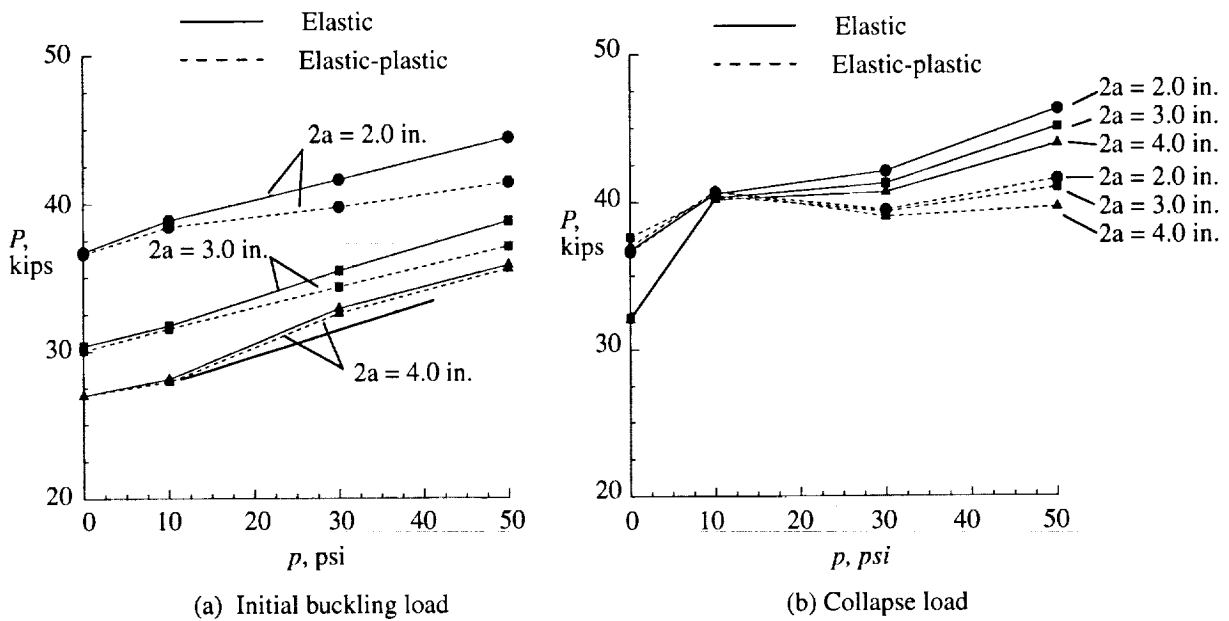
(b) Collapse load

Figure 18. Initial buckling load and collapse load as a function of internal pressure and initial crack length for a 0.040-inch-thick shell subjected to combined internal pressure and axial compression loads.

(a) Load-shortening response

(b) Magnified view of local and global buckling points
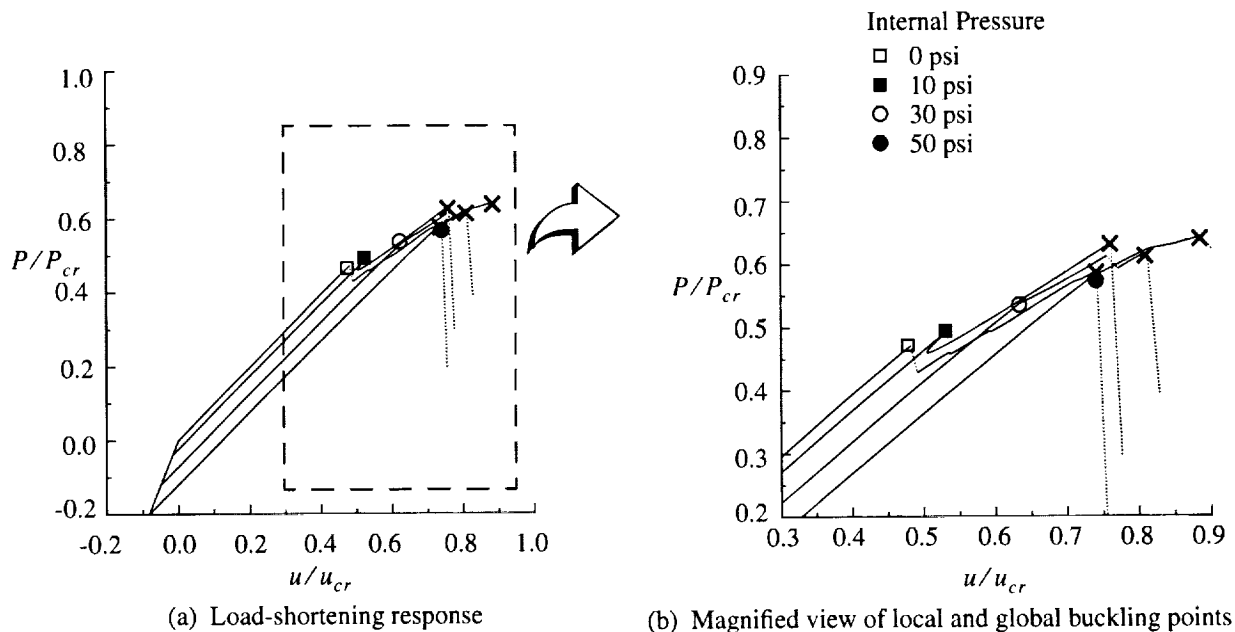
Figure 19. Predictions from an elastic-plastic analysis of the effect of internal pressure on the load-shortening response of a 0.040-inch-thick shell with a 3.0-inch-long longitudinal crack.

(a) Initial postbuckling deformation pattern

(b) General instability deformation pattern
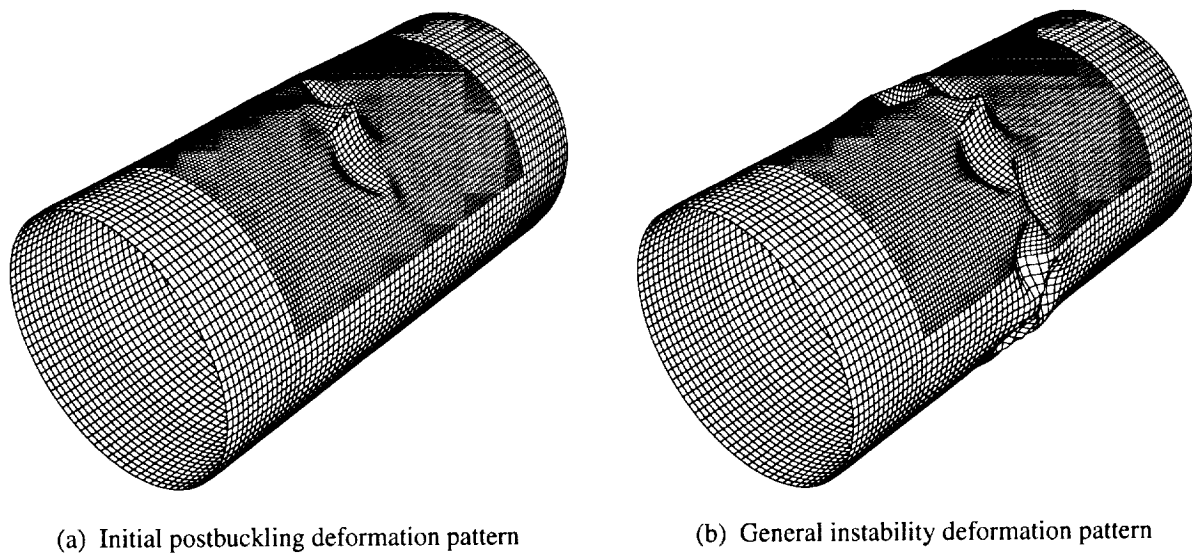
Figure 20. Selected deformation patterns for a 0.040-inch-thick shell with a 3.0-inch-long longitudinal crack and subjected to 30 psi of internal pressure and an axial compression load.
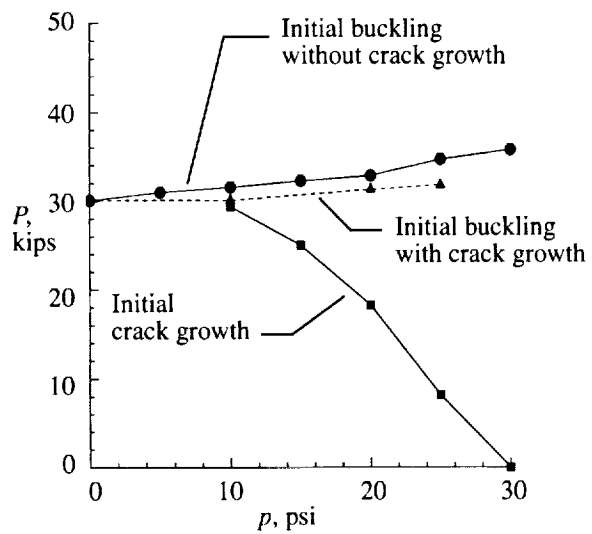
Figure 21. Interaction between crack growth and
          initial buckling for a 0.040-inch-thick
          shell with a 3.0-inch-long crack and
          subjected to combined internal
          pressure and axial compression loads.

American Institute of Aeronautics and Astronautics